Progress In Electromagnetics Research M, Vol. 107, 131–140, 2022

Analytical and Numerical Studies of Oblique Wave Incidence on Impedance-Matched Graded Interfaces between RHM and LHM Media

Brage B. Svendsen*, Balwan Rana, and Mariana Dalarsson

Abstract—This paper presents analytical and numerical studies of electromagnetic wave propagation through an interface between a regular right-handed material (RHM) and a left-handed metamaterial (LHM). The interface is graded along the direction perpendicular to the boundary plane between the two materials, chosen to be the x-direction. The permittivity $\varepsilon(\omega, x)$ and permeability $\mu(\omega, x)$ are chosen to vary according to hyperbolic tangent functions. We show that the field intensities for both TE- and TM-cases satisfy the same differential equations, and we obtain remarkably simple exact analytical solutions to Helmholtz' equations for lossy media. The obtained exact analytical results for the field intensities along the graded RHM-LHM composite confirm all the expected properties of RHM-LHM structures. Finally, we perform a numerical study of the wave propagation over an impedance-matched graded RHM-LHM interface, using the software COMSOL Multiphysics, and obtain an excellent agreement between the numerical simulations and analytical results. The results obtained in the present paper are not limited to any particular application, and are generally useful for all cases of wave propagation over impedance-matched two- and three-dimensional interfaces between RHM and LHM media. The advantage of the present method is that it can model smooth realistic material transitions, while at the same time including the abrupt transition as a limiting case. Furthermore, unlike previously existing solutions, the interface width is included as a parameter in the analytical solutions in a very simple way. This enables the use of the interface width as an additional degree of freedom in the design of practical RHM-LHM interfaces.

1. INTRODUCTION

In the last two decades, there has been an increasing theoretical and experimental interest in graded RHM-LHM structures [1, 2] where permittivities and permeabilities are spatially varying according to suitably chosen continuous functions. Spatially varying permittivities and permeabilities are useful in a number of areas of scientific interest [3–6, 10–18, 22–24]. One such major area is transformation optics [25], with unprecedented design flexibility allowing for creation of of novel devices, such as light source collimators, waveguide adapters and waveguide crossings, useful in integrated photonic chips and compatible with modern fabrication technology. The superior optical performance of the abovementioned devices, along with their efficient integration with other components in an on-chip photonic system, is numerically confirmed in [25]. Transformation optics-based components require spatially-varying dielectric materials only, with no specific magnetic properties. This enables their use in low-loss, broadband and integrated photonic applications.

Other applications of transformation optics include hyperlenses [4, 26], specialized antennas [5, 6, 10–18], as well as subwavelength imaging [7, 9]. In [26], an ultracompact, robust, and efficient

Received 27 November 2021, Accepted 6 January 2022, Scheduled 12 January 2022
* Corresponding author: Brage B. Svendsen (bragebs@kth.se).
The authors are with the Division of Electromagnetic Engineering, KTH Royal Institute of Technology, SE-100 44 Stockholm, Sweden.

spot size converter with a gradient-index (GRIN) profile is discussed. The proposed GRIN-lens-assisted spot size converter provides an unprecedented combination of reduced footprint and insertion losses, as well as large bandwidth and tolerance to fabrication errors. In [4], a dielectric metamaterial-based GRIN lens in the terahertz frequency range is studied, showing that GRIN metamaterials are suitable for designing photonic components (metadevices) for applications at terahertz frequencies. In [6], a flat transformation-optics high-gain GRIN-lens antenna with multiple polarizations and beam scanning ability, useful for remote sensing and far-field imaging applications, is reported. Far-field subwavelength imaging using phase-gradient metasurfaces is studied in [7], using the capability of metamaterials to convert evanescent waves to propagating waves. Similar principles are used in [9] for far-field superlensing inside biological media through a nanorod lens. In [10], a comprehensive survey of metamaterial transmission-line based antennas is given, while in [11], a comprehensive survey of decoupling mechanisms with focus on metamaterial and metasurface principles applicable to SAR and MIMO antenna systems is given. More details on these applications can be found in [12–18].

A further area of interest is within waveguide applications [8, 22]. Particularly interesting are the nanostructured waveguides which are expected to improve the performance of solar cells using a tunable absorption spectrum [23].

Yet another area of interest is electromagnetic cloaking. The principles of transformation optics with metamaterials are considered as key enablers for the possibility to manipulate surface waves, in particular, towards the THz and optical regime. In [24], a surface wave cloak, using engineered GRIN materials, has been experimentally demonstrated, showing the possibility of using nanocomposites to control surface wave propagation. In [5], a compact high-performance lens antenna, based on impedance-matching GRIN metamaterials is studied. The designed lens is composed of isotropic but inhomogeneous metamaterials that can provide impedance matching with free space. A few other examples of impedance-matched devices based on electromagnetic metamaterials can be found in [19–21]. In conclusion, the interest in impedance-matched GRIN metamaterials is growing in many applications, with an increasing need for general analytical and numerical studies of impedance-matched metamaterial composites.

In this paper, we study electromagnetic wave propagation over an impedance-matched graded RHM-LHM structure. A similar investigation was partly performed by one of the present authors in [27] concerning the lossless case of oblique TE-wave incidence on an impedance matched graded RHM-LHM interface. The special case of normal incidence on an impedance matched graded RHM-LHM interface has been reported in [28]. A general approach to a non-impedance-matched graded RHM-LHM interface has been presented in [29]. In [27], the analytical solution was derived in terms of Gaussian hypergeometric functions. Gaussian hypergeometric functions are mathematically complex, and solutions based on them are not always easy to visualize. Therefore, in an early study like [27], the field patterns were not studied in detail and properly presented to highlight the important properties of LHM-media.

In the present paper, the exact analytical solution from [27] is successfully reduced to a solution involving elementary mathematical functions only, by means of a number of properties of Gaussian hypergeometric functions [31]. Furthermore, the exact analytical solutions presented here are generalized to a lossy case and to both TE- and TM-waves, where we show that the field intensities for TE- and TM-cases satisfy the same differential equations. We thereby obtain remarkably simple exact analytical solutions to Helmholtz' equations in lossy cases with hyperbolic tangent permittivity and permeability profiles. We provide three-dimensional graphical presentations of these solutions, and discuss the obtained results from the point of view of well-known properties of LHM-media.

Last but not least, we perform a numerical study of the wave propagation over the impedance-matched graded RHM-LHM interface, using the COMSOL software. An excellent agreement is obtained between the numerical simulations and analytical results.

2. FIELD EQUATIONS WITH SOLUTIONS

In the present paper, we describe the RHM-LHM composite by its graded effective dielectric permittivity $\varepsilon(\omega, x)$ and its effective magnetic permeability $\mu(\omega, x)$. Such a description is normally justified for left-handed metamaterials, since their 'particles' have subwavelength dimensions. We choose the geometry

of the problem such that the effective parameters change along one direction only (chosen to be the x-axis). The plane of incidence is chosen to be x-y plane, such that the direction perpendicular to the plane of incidence is the z-direction. As shown in [27] for a TE-wave, with an oblique incidence at angle θ, the magnetic and electric field vectors are given respectively by

$$\mathbf{E}(x,y) = -E(x,y)\hat{\mathbf{z}}, \quad \mathbf{H}(x,y) = -H(x,y)\sin\theta\hat{\mathbf{x}} + H(x,y)\cos\theta\hat{\mathbf{y}} \tag{1}$$

On the other hand, for a TM-wave, with an oblique incidence at angle θ, the magnetic and electric field vectors are given respectively by

$$\mathbf{H}(x,y) = H(x,y)\hat{\mathbf{z}}, \quad \mathbf{E}(x,y) = -E(x,y)\sin\theta\hat{\mathbf{x}} + E(x,y)\cos\theta\hat{\mathbf{y}} \tag{2}$$

In both cases, the incident wave vector is $\mathbf{k} = k\cos\theta\hat{\mathbf{x}} + k\sin\theta\hat{\mathbf{y}}$, where k is the complex-valued wave vector length in lossy media. It turns out that the electric field intensity $E(x,y)$ and magnetic field intensity $H(x,y)$ satisfy the following differential equations

$$\frac{\partial^2 E}{\partial x^2} + \frac{\partial^2 E}{\partial y^2} - \frac{1}{\mu}\frac{\mathrm{d}\mu}{\mathrm{d}x}\frac{\partial E}{\partial x} + \omega^2\varepsilon\mu E = 0, \quad \frac{\partial^2 H}{\partial x^2} + \frac{\partial^2 H}{\partial y^2} - \frac{1}{\varepsilon}\frac{\mathrm{d}\varepsilon}{\mathrm{d}x}\frac{\partial H}{\partial x} + \omega^2\varepsilon\mu H = 0 \tag{3}$$

For the lossy impedance-matched graded interface between a right-handed material (RHM) and a left-handed material (LHM), it is convenient to define the permittivity and permeability functions, changing according to a hyperbolic tangent function along the x-direction, as follows

$$\varepsilon(\omega,x) = -\varepsilon_0\varepsilon_R(\omega)\left[\tanh\left(\frac{x}{x_0}\right) + \mathrm{i}\beta\right], \quad \mu(\omega,x) = -\mu_0\mu_R(\omega)\left[\tanh\left(\frac{x}{x_0}\right) + \mathrm{i}\beta\right] \tag{4}$$

where x_0 is the length parameter that defines the width of the graded transition region between the two media, and $\varepsilon_R(\omega)$ and $\mu_R(\omega)$ are the real parts of the relative permittivity and permeability, respectively. The loss parameter β is the ratio between imaginary and real parts of the permittivity and permeability functions defined in Eq. (4). This parameter is assumed to be equal and a good approximation constant for the chosen dispersion model in the frequency range of interest. It is here useful to introduce the wave-vector parameter k, whose square is defined by

$$k^2 = \omega^2\varepsilon_0\mu_0\varepsilon_R(\omega)\mu_R(\omega) = \frac{\omega^2}{c^2}\varepsilon_R(\omega)\mu_R(\omega) \tag{5}$$

The two differential equations (3) are solved by separation of variables, using $E(x,y) = X(x)Y(y)$ and $H(x,y) = X(x)Y(y)$, respectively. Following [27], using $E(x,y) = X(x)Y(y)$, we obtain

$$\frac{\mathrm{d}^2 X}{\mathrm{d}x^2} - \frac{1}{\mu}\frac{\mathrm{d}\mu}{\mathrm{d}x}\frac{\mathrm{d}X}{\mathrm{d}x} + \left(\omega^2\varepsilon\mu - k_y^2\right)X = 0, \quad \frac{\mathrm{d}^2 Y}{\mathrm{d}y^2} + k_y^2 Y = 0 \tag{6}$$

The solution for $Y(y)$ is a simple attenuated plane wave $Y(y) = \exp(\pm\mathrm{i}k_y y)$, where $k_y = k\sin\theta$. Using the procedure outlined in [27], the ordinary differential equation for $X(x)$ is reduced to the hypergeometric differential equation, with a solution proportional to a Gaussian hypergeometric function ${}_2F_1(a,b,c;u)$. Thus, in a lossless case, up to a multiplicative constant X_0, the following solution was obtained in [27]

$$\begin{aligned} X(x) \;=\; & X_0\left(\mathrm{e}^{x/x_0} + \mathrm{e}^{-x/x_0}\right)^{\mathrm{i}kx_0\cos\theta}\tanh^2(x/x_0) \\ & \times {}_2F_1\left[1 + \mathrm{i}\frac{kx_0}{2}(\cos\theta+1), 1 + \mathrm{i}\frac{kx_0}{2}(\cos\theta-1), 2; \tanh^2(x/x_0)\right] \end{aligned} \tag{7}$$

However, in the present study, we have generalized the solution for $X(x)$ to include losses in the structure. Further, using the properties of Gaussian hypergeometric functions [31], we have successfully reduced the solution for $X(x)$ to the one that involves elementary mathematical functions only. Thus, the complete exact analytical solution for $E(x,y)$ has the following simple form

$$E(x,y) = E_0 e^{-\beta k(x\cos\theta + y\sin\theta)} \cdot \left[\cosh\left(\frac{x}{x_0}\right)\right]^{\mathrm{i}kx_0\cos\theta} e^{-\mathrm{i}ky\sin\theta} \tag{8}$$

where we introduce the notation E_0 for the electric field strength at the origin $(x, y) = (0, 0)$. The solution for the magnetic field strength $H(x, y)$ is proportional to the solution for the electric field strength $E(x, y)$, and has a fully analogous mathematical form

$$H(x,y) = H_0 e^{-\beta k(x\cos\theta + y\sin\theta)} \cdot \left[\cosh\left(\frac{x}{x_0}\right)\right]^{\mathrm{i}kx_0\cos\theta} e^{-\mathrm{i}ky\sin\theta} \tag{9}$$

where H_0 is the magnetic field strength at $(x, y) = (0, 0)$. In the two field solutions (8) and (9), the dependency on the material parameters, defined by the frequency-dependent functions $\varepsilon_R(\omega)$ and $\mu_R(\omega)$ in Eq. (4), is not explicit. The material parameters enter the solutions (8) and (9) only implicitly via the wave-vector parameter k, whose square is defined in Eq. (5) as a function of $\varepsilon_R(\omega)$ and $\mu_R(\omega)$.

3. GRAPHICAL PRESENTATION OF THE ANALYTICAL RESULTS

We present the analytical electric field intensity pattern $E(x, y)$ defined by Eq. (8) for the microwave range of frequencies in Figure 1. The images included in Figure 1 have the following properties: the

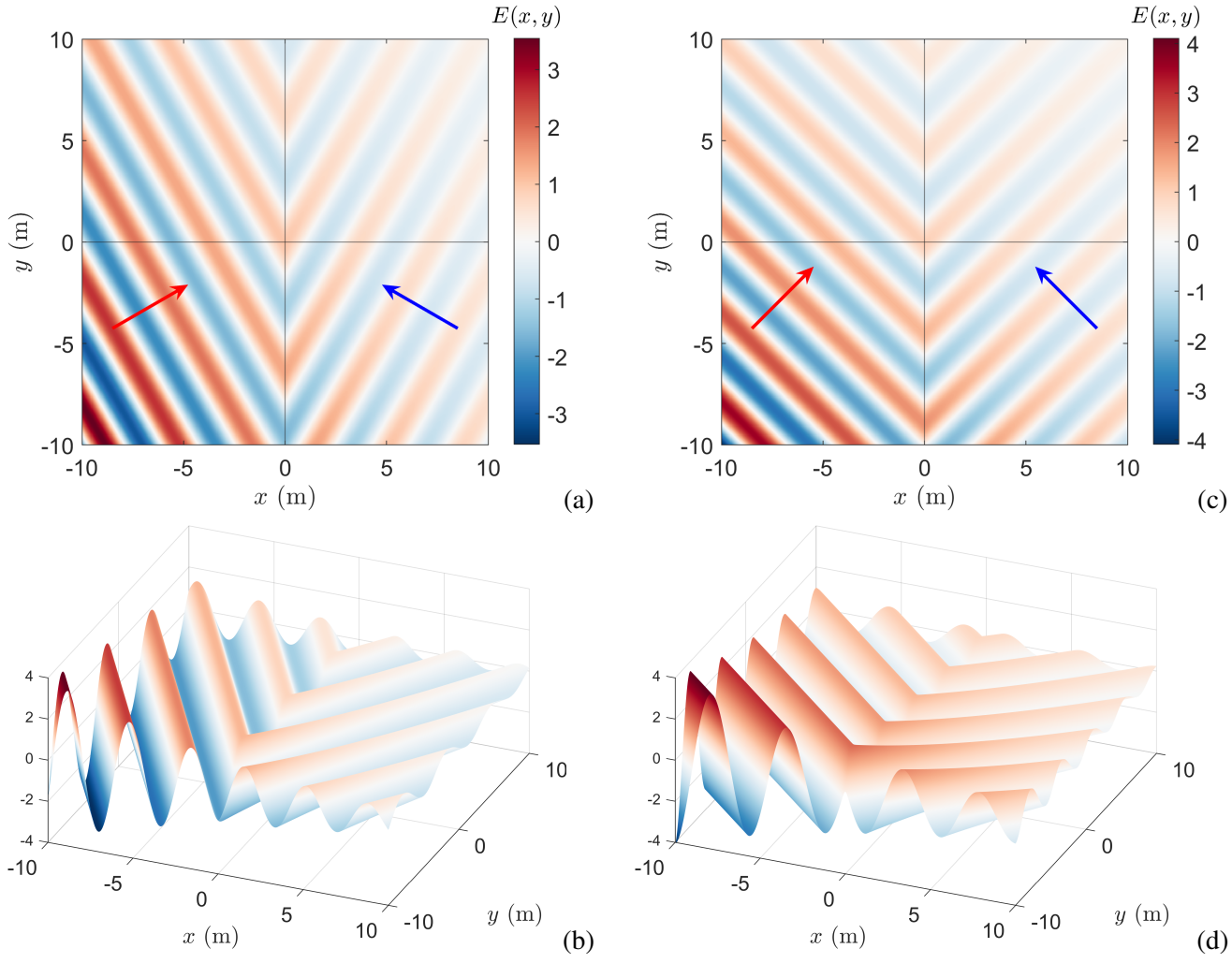

Figure 1. Exact analytical electric field intensity pattern for $E_0 = 1\,\mathrm{V/m}$, $kx_0 = 0.2$, $x_0 = 0.1\,\mathrm{m}$ and $\beta = 0.05$, with angles of incidence (a) $\theta = \pi/6$ and (c) $\theta = \pi/4$. The arrows indicate wave vector directions for RHM (red) and LHM (blue). The 2D and 3D representations of incidence angle $\theta = \pi/6$ are shown in (a)–(b), while the corresponding results for $\theta = \pi/4$ are shown in (c)–(d).

normalization amplitude at the origin $E_0 = 1\,\mathrm{V/m}$, the wave number k such that $kx_0 = 0.2$, the transition region length $x_0 = 0.1\,\mathrm{m}$, and the loss factor $\beta = 0.05$. The results display the wave propagation between the RHM and LHM with the angle of incidence (a)–(b) $\theta = \pi/6$ and (c)–(d) $\theta = \pi/4$. Figure 1 shows the 2D representation of the wave propagation in (a) and (c), while the 3D representation of the wave propagation is shown in (b) and (d).

4. NUMERICAL MODEL AND RESULTS

The finite element method software COMSOL Multiphysics was used to model a lossy impedance-matched graded interface between RHM and LHM media. A two-dimensional square geometry was deployed with ports on opposing sides of the x-axis, backed by perfectly matched layers. The material properties were described in agreement with the analytical functions (4), such that the wave excitation occurred on the port located in the RHM and propagated towards the LHM at an angle θ. The top and bottom boundaries were given periodic Floquet boundary conditions to simulate a domain stretching infinitely in y-direction. As we already argued before, the field intensities for the TM and TE waves are the same. It was therefore in principle possible to choose either of the two polarizations for the purposes

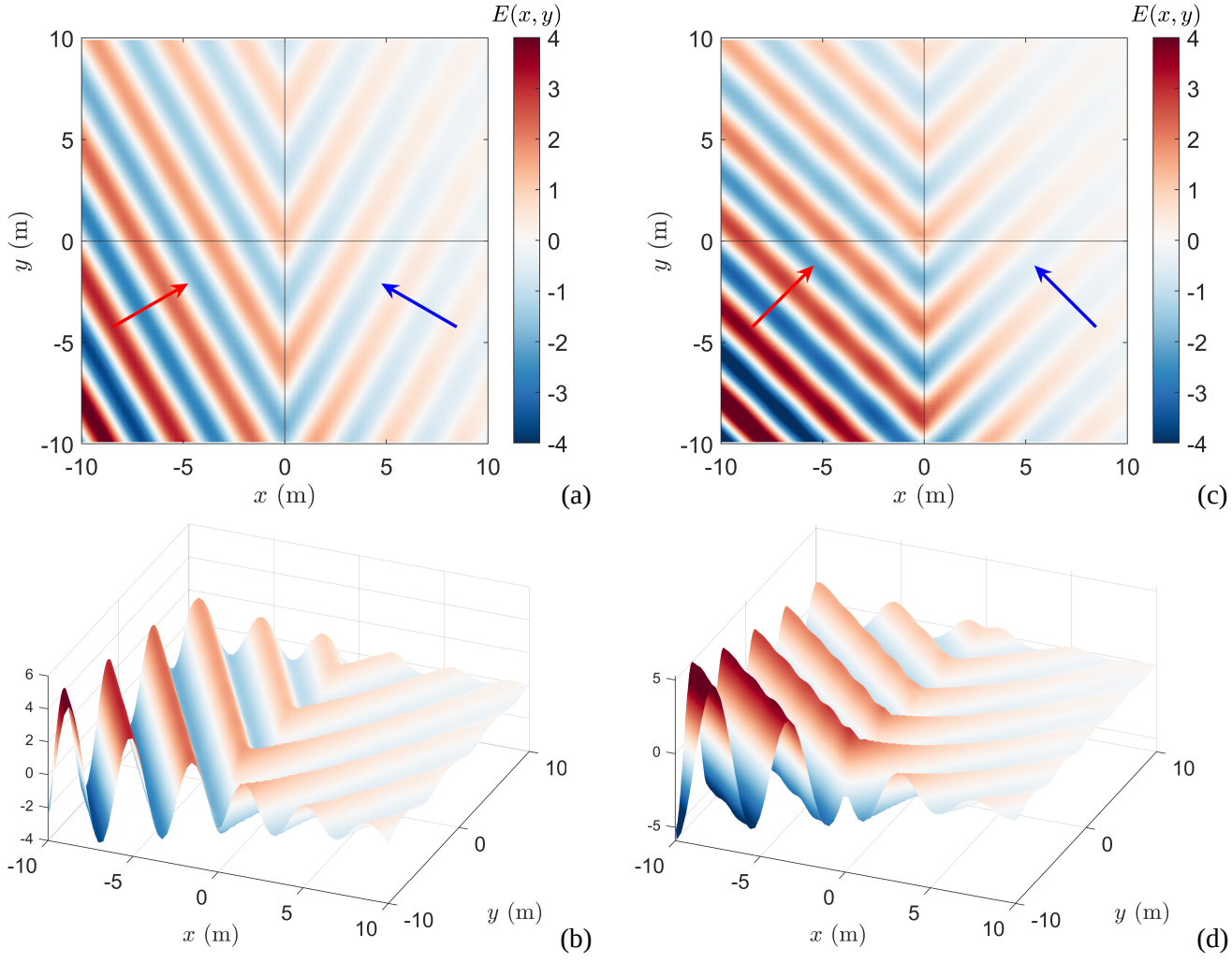

Figure 2. Numerically obtained electric field intensity pattern for $E_0 = 1$, $kx_0 = 0.2$, $x_0 = 0.1$ m and $\beta = 0.05$, with angles of incidence (a) $\theta = \pi/6$ and (b) $\theta = \pi/4$. Arrows indicate wave vector directions for RHM (red) and LHM (blue). The 2D and 3D representations of incidence angle $\theta = \pi/6$ are shown in (a)–(b), while the corresponding results for $\theta = \pi/4$ are shown in (c)–(d).

of numerical simulation using COMSOL. In the simulations presented here, the TM-polarization was used.

Thus, we here present the numerical electric field intensity pattern $E(x, y)$ for a TM-wave in the microwave range of frequencies in Figure 2. The field values are normalized with respect to its value at the origin $E(0, 0)$ so that $E_0 = 1$. The wave number k is chosen such that $kx_0 = 0.2$, the loss factor is $\beta = 0.05$, and the angle of incidence is (a)–(b) $\theta = \pi/6$ and (c)–(d) $\theta = \pi/4$. Similarly as for Figure 1, the bottom plots of Figure 2 visualize the 3D electric field wave pattern across the geometry.

The cross section of the electric field pattern shown in Figure 2 for constant $y = \pi/2$ is shown in Figure 3, with otherwise the same parameters as the previous two figures. The function shown in Figure 3 describes the wave propagation along the x-axis only for the angle $\theta = \pi/6$.

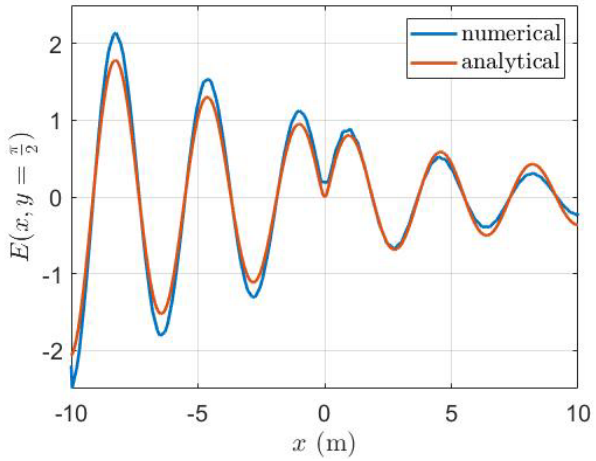

Figure 3. Electric field pattern along $y = \pi/2$ with $E_0 = 1$, $kx_0 = 0.2$, $x_0 = 0.1\,\mathrm{m}$, $\beta = 0.05$ and $\theta = \pi/6$.

5. DISCUSSION

For normal incidence, when $\theta = 0$, in the lossless case with $\beta = 0$, the result in Eq. (8) is reduced to the previously obtained result in [30]

$$E(x) = E_0 \left[\cosh\left(\frac{x}{x_0}\right)\right]^{\mathrm{i}kx_0} \tag{10}$$

The result in Eq. (10) was validated by comparison of the exact analytical waveforms with the corresponding waveforms obtained by simulation using COMSOL, in Figure 3 in [30].

In the impedance-matched case, as the one studied here and in [27, 28, 30], there is no reflection at the interface between the two media. In the case of normal incidence, described by Eq. (10), it means that the wave seemingly continues to propagate undisturbed over the boundary between the two media. However, one important physical observation is the reversed sign of the wave vector in the left-handed media, being a well-known property of LHM media. Thus, in the special case of normal incidence, the wave continues to propagate over the boundary between two very different media, and only changes the sign of the wave vector (direction of wave vector along the same straight line).

On the other hand, for oblique incidence, the wave vector $\mathbf{k} = k\cos\theta\hat{\mathbf{x}} + k\sin\theta\hat{\mathbf{y}}$ has both x- and y-components. And since the media change from RHM to LHM occurs only in the x-direction, only the sign of the x-component of the wave vector is changed, while the sign of the y-component is unchanged. Thus in Figures 1–3, we see that despite the impedance-matching and no wave reflection at the boundary between the two materials, the incident electromagnetic wave does not continue along the same path in the LHM medium.

Wave refraction occurs at the boundary between the two materials, and the wave not only propagates in the opposite direction from what is expected in RHM media, but also propagates along a path that is a mirror image of the incident wave. This observation can be interpreted as an RHM-LHM interface version of Snell's law of refraction $n_t \sin\theta_t = n_i \sin\theta_i$, where $n_t = -n_i$ is the negative refractive index of the left-handed material while n_i is the positive refractive index of the right-handed material. Thus, $\sin\theta_t = -\sin\theta_i$ which implies $\theta_t = -\theta_i$, in agreement with the behavior established in the present analysis. This peculiar property of LHM media may have implications for some invisibility cloaking designs.

It should be emphasized however that in the present treatment, we do not need to use any law of refraction, or any boundary conditions. The solution of Maxwell's equations for a stratified medium consisting of an RHM-LHM composite reproduces the correct LHM media behavior without any a priori assumptions. The stratified model includes also the case of abrupt transition, i.e., a sharp interface between the two materials, as a special case when the width of transition region x_0 approaches zero ($x_0 \to 0$). Far from the boundary surface between the two media, the result in Eq. (8) with $\beta = 0$ reproduces the expected asymptotic plane-wave solutions for $x \to -\infty$

$$E(x,y) = E_0 e^{-\mathrm{i}\alpha} e^{-\mathrm{i}\mathbf{k}_i\cdot\mathbf{x}} = E_0 e^{-\mathrm{i}\alpha} e^{-\mathrm{i}(kx\cos\theta + ky\sin\theta)} \tag{11}$$

and for $x \to +\infty$

$$E(x,y) = E_0 e^{-\mathrm{i}\alpha} e^{-\mathrm{i}\mathbf{k}_t\cdot\mathbf{x}} = E_0 e^{-\mathrm{i}\alpha} e^{-\mathrm{i}(-kx\cos\theta + ky\sin\theta)} \tag{12}$$

where $\mathbf{k}_i$ and $\mathbf{k}_t$ are complex wave vectors in RHM and LHM media, respectively, and $\alpha = kx_0 \ln 2 \cos\theta$ is an unessential constant phase shift that can be included in a complex amplitude E_0. These asymptotic results reconfirm that the directions of two wave vectors in the two media are indeed in agreement with the wave behavior displayed in Figures 1 and 3.

The numerical results obtained from simulation in COMSOL show an excellent agreement with the analytical results presented in Section 3 above. If we examine Figures 2 and 3, there are slight fluctuations of the propagating wave inside the medium. These phenomena are believed to originate from the handling of the gradient transition phase between the RHM and LHM media by COMSOL. Small amplitude deviations are observed in Figure 3 throughout the medium. These deviations are related to the slight inaccuracy in the choice of the excitation power at the port, as well as to the finite size in x-direction of the RHM-LHM composite as defined in COMSOL.

Finally, it is of interest to compare the present results to the results reported earlier in [29] and [30]. In [29], the most general approach to unbounded non-impedance-matched graded RHM-LHM composites was reported. In principle, it includes the results presented here as a special case. However, as explained in the introduction, the general approach in [29] leads to analytical solutions in terms of mathematically complex Gaussian hypergeometric functions. For practical purposes, it is always valuable to reduce the complexity of analytical solutions, which can only be done in certain special cases, like in the case of an unbounded impedance-matched RHM-LHM composite studied in the present paper. For example, the new lossy field solution (8), involving elementary functions only, represents an improvement in our understanding of the wave propagation phenomena in RHM-LHM composites, compared to the previously obtained lossless solution $E(x,y) = X(x)Y(y)$, with $X(x)$ defined by Eq. (7). Regarding the results reported in [30], they were limited to lossless media and normal incidence only. LHMs are generally lossy, and it is of interest to extend our understanding to lossy media. The present results are valid for oblique incidence of both TE- and TM-waves, and include losses in the composite. This constitutes a qualitative improvement of our understanding of wave propagation phenomena in unbound RHM-LHM composites. Last but not the least, in the present paper, we perform a numerical study, make a structured presentation of both analytical and numerical results, and discuss some important LHM-properties, none of which was done in [29] and [30].

6. CONCLUSIONS

We presented analytical and numerical studies of electromagnetic wave propagation over an infinite RHM-LHM composite, graded along the direction perpendicular to the boundary plane between the two materials. The permittivity $\varepsilon(\omega, x)$ and permeability $\mu(\omega, x)$ varied according to hyperbolic tangent functions along the x-direction. We showed that the electric and magnetic field intensities, for both the

TE- and TM-case, satisfy the same Helmholtz' equations for lossy media. We presented remarkably simple exact analytical solutions for the field intensities, which confirm all the expected properties of RHM-LHM structures. Finally, we performed a numerical study of the wave propagation over an impedance-matched graded RHM-LHM interface, using the COMSOL Multiphysics software, and obtained an excellent agreement between the numerical simulations and analytical results.

ACKNOWLEDGMENT

The work of M. D. is supported by the Swedish Research Council (VR) under project number 2018-05001.

REFERENCES

1. Smith, D. R., J. J. Mock, A. F. Starr, and D. Schurig, "A gradient index metamaterial," *Phys. Rev. E*, Vol. 71, 036609, March 2005, doi: 10.1103/PhysRevE.71.036609.
2. Litchinitser, N. M., A. I. Maimistov, I. R. Gabitov, R. Z. Sagdeev, and V. M. Shalaev, "Metamaterials: Electromagnetic enhancement at zero-index transition," *Optics Letters*, Vol. 33, No. 20, 2350–2352, 2008, doi: 10.1364/OL.33.002350.
3. Pinchuk, A. O. and G. C. Schatz, "Metamaterials with gradient negative index of refraction," *Journal of the Optical Society of America A*, Vol. 24, No. 10, A39–A44, 2007, doi: 10.1364/JOSAA.24.000A39.
4. Gaufillet, F., S. Marcellin, and E. Akmansoy, "Dielectric metamaterial-based gradient index lens in the terahertz frequency range," *IEEE Journal of Selected Topics in Quantum Electronics*, Vol. 23, No. 4, 1–5, July/August 2017, Art no. 4700605, doi: 10.1109/JSTQE.2016.2633825.
5. Zhang, N., W. X. Jiang, H. F. Ma, W. X. Tang, and T. J. Cui, "Compact high-performance lens antenna based on impedance-matching gradient-index metamaterials," *IEEE Transactions on Antennas and Propagation*, Vol. 67, No. 2, 1323–1328, February 2019, doi: 10.1109/TAP.2018.2880115.
6. Su, Y. and Z. N. Chen, "A flat dual-polarized transformation-optics beamscanning Luneburg lens antenna using PCB-stacked gradient index metamaterials," *IEEE Transactions on Antennas and Propagation*, Vol. 66, No. 10, 5088–5097, October 2018, doi: 10.1109/TAP.2018.2858209.
7. Salami, P. D. and L. Yousefi, "Far-field subwavelength imaging using phase gradient metasurfaces," *IEEE Journal of Lightwave Technology*, Vol. 37, No. 10, 2317–2323, March 2019, doi: 10.1109/JLT.2019.2902544.
8. Badri, S. H., H. R. Saghai, and H. Soofi, "Multimode waveguide crossing based on a square Maxwell's fisheye lens," *Applied Optics*, Vol. 58, No. 17, 4647–4653, June 2019, doi: 10.1364/AO.58.004647.
9. Hajiahmadi, M. J., R. Faraji-Dana, and A. K. Skrivervik, "Far field superlensing inside biological media through a nanorod lens using spatiotemporal information," *Nature, Scientific Reports*, Vol. 11, 1–8, January 2021, Art no. 19534, doi: 10.1038/s41598-021-81091-0.
10. Alibakshikenari, M., B. S. Virdee, L. Azpilicueta, M. Naser-Moghadasi, M. Olusola Akinsolu, C. H. See, B. Liu, R. A. Abd-Alhameed, F. Falcone, I. Huynen, T. A. Denidni, and E. Limiti, "A comprehensive survey of metamaterial transmission-line based antennas: Design, challenges, and applications," *IEEE Access*, Vol. 8, 144778–144808, August 2020, doi: 10.1109/ACCESS.2020.3013698.
11. Alibakshikenari, M., F. Babaeian, S. Aïssa, C. H. See, A. A. Althuwayb, I. Huynen, R. A. Abd-Alhameed, F. Falcone, and E. Limiti, "A comprehensive survey on various decoupling mechanisms with focus on metamaterial and metasurface principles applicable to SAR and MIMO antenna systems," *IEEE Access*, Vol. 8, 192965–193004, November 2020, doi: 10.1109/ACCESS.2020.3032826.

12. Alibakhshikenari, M., B. S. Virdee, and E. Limiti, "Compact single-layer traveling-wave antenna design using metamaterial transmission lines," *Radio Science*, Vol. 52, 1510–1521, December 2017, doi: 10.1002/2017RS006313.
13. Alibakhshi-Kenari, M., M. Naser-Moghadasi, R. A. Sadeghzadeh, B. S. Virdee, and E. Limiti, "Periodic array of complementary artificial magnetic conductor metamaterials-based multiband antennas for broadband wireless transceivers," *IET Microwaves, Antennas & Propagation*, Vol. 10, No. 15, 1682–1691, June 2016, doi: 10.1049/iet-map.2016.0069.
14. Alibakhshi-Kenari, M., M. Naser-Moghadasi, and R. A. Sadeghzadeh, "Bandwidth and radiation specifications enhancement of monopole antennas loaded with split ring resonators," *IET Microwaves, Antennas & Propagation*, Vol. 9, No. 14, 1487–1496, May 2015, doi: 10.1049/iet-map.2015.0172.
15. Alibakhshi-Kenari, M., M. Naser-Moghadasi, and R. A. Sadeghzadeh, "Composite right-left-handed-based antenna with wide applications in very-high frequency-ultra-high frequency bands for radio transceivers," *IET Microwaves, Antennas & Propagation*, Vol. 9, No. 15, 1713–1726, July 2015, doi: 10.1049/iet-map.2015.0308.
16. Alibakhshi-Kenari, M., M. Naser-Moghadasi, R. A. Sadeghzadeh, and B. S. Virdee, "Metamaterial-based antennas for integration in UWB transceivers and portable microwave handsets," *International Journal of RF and Microwave Computer-Aided Engineering*, Vol. 26, No. 1, 88–96, January 2016, doi: 10.1002/mmce.20942.
17. Alibakhshi-Kenari, M., M. Naser-Moghadasi, and R. Sadeghzadeh, "The resonating MTM-based miniaturized antennas for wide-band RF-microwave systems," *Microwave and Optical Technology Letters*, Vol. 57, No. 10, 2339–2344, October 2015, doi: 10.1002/mop.29328.
18. Alibakhshikenari, M., B. S. Virdee, A. Ali, and E. Limiti, "A novel monofilar-Archimedean metamaterial inspired leaky-wave antenna for scanning application for passive radar systems," *Microwave and Optical Technology Letters*, Vol. 60, No. 10, 2055–2060, February 2018, doi: 10.1002/mop.31300.
19. Alibakshikenari, M., B. S. Virdee, P. Shukla, Y. Wang, L. Azpilicueta, M. Naser-Moghadasi, C. H. See, I. Elfergani, C. Zebiri, R. A. Abd-Alhameed, I. Huynen, J. Rodriguez, T. A. Denidni, F. Falcone, and E. Limiti, "Impedance bandwidth improvement of a planar antenna based on metamaterial-inspired T-matching network," *IEEE Access*, Vol. 9, 67916–67927, May 2021, doi: 10.1109/ACCESS.2021.3076975.
20. Alibakhshikenari, M., B. S. Virdee, C. H. See, R. A. Abd-Alhameed, F. Falcone, and E. Limiti, "Impedance matching network based on metasurfaces (2-D metamaterials) for electrically small antennas," *2020 IEEE International Symposium on Antennas and Propagation and North American Radio Science Meeting*, 1953–1954, 2020, doi: 10.1109/IEEECONF35879.2020.9330460.
21. Alibakhshikenari, M., B. S. Virdee, P. Shukla, C. H. See, R. A. Abd-Alhameed, F. Falcone, and E. Limiti, "Improved adaptive impedance matching for RF front-end systems of wireless transceivers," *Scientific Reports*, Vol. 10, 14065, 2020, doi: 10.1038/s41598-020-71056-0.
22. Fu, Y., Y. Xu, and H. Chen, "Applications of gradient index metamaterials in waveguides," *Nature, Scientific Reports*, Vol. 5, 1–6, December 2015, Art no. 18223, doi: 10.1038/srep18223.
23. El-Khozondar, H. J., R. J. El-Khozondar, A. Shama, K. Ahmed, and V. Dhasarathan, "Highly efficient solar energy conversion using graded-index metamaterial nanostructured waveguide," *Journal of Optical Communications*, eISSN 2191-6322, ISSN 0173-4911, February 2020, doi: 10.1515/joc-2019-0285.
24. La Spada, L., T. M. McManus, A. Dyke, S. Haq, L. Zhang, Q. Cheng, and Y. Hao, "Surface wave cloak from graded refractive index nanocomposites," *Nature: Scientific Reports*, Vol. 6, 29363, July 2016, doi: 10.1038/srep29363.
25. Wu, Q., J. P. Turpin, and D. H. Werner, "Integrated photonic systems based on transformation optics enabled gradient index devices," *Nature, Light: Science & Applications*, Vol. 1, 1–6, November 2012, Art no. 4700605, doi: 10.1038/lsa.2012.38.

26. Luque-González, J. M., R. Halir, J. G. Wanguemert-Perez, J. de-Oliva-Rubio, J. H. Schmid, P. Cheben, Í. Molina-Fernandez, and A. Ortega-Monux, "An ultracompact GRIN-lens-based spot size converter using subwavelength grating metamaterials," *Laser Photonics Reviews*, Vol. 13, 1–7, September 2019, doi: 10.1002/lpor.201900172.
27. Dalarsson, M., Z. Jaksic, and P. Tassin, "Exact analytical solution for oblique incidence on a graded index interface between a right-handed and a left-handed material," *Journal of Optoelectronics and Biomedical Materials*, Vol. 1, No. 4, 345–352, December 2009.
28. Dalarsson, M., M. K. Norgren, T. Asenov, and N. Doncov, "Arbitrary loss factors in the wave propagation between RHM and LHM media with constant impedance throughout the structure," *Progress In Electromagnetics Research*, Vol. 137, 527–538, 2013.
29. Dalarsson, M., "General theory of wave propagation through graded interfaces between positive- and negative refractive-index media," *Physical Review A*, Vol. 96, 043848, October 2017, doi: PhysRevA.96.043848.
30. Dalarsson, M. and P. Tassin, "Analytical solution for wave propagation through a graded index interface between a right-handed and a left-handed material," *Optics Express*, Vol. 17, 6747–6752, April 2009.
31. Abramowitz, M. and I. A. Stegun, *Handbook of Mathematical Functions: With Formulas, Graphs, and Mathematical Tables*, Dover Books, New York, 1965.